Pergamon

PII: S0301-9322(96)00059-6

Int. J. Multiphase Flow Vol. 23, No. 1, pp. 93–111, 1997

0301-9322/97 $17.00 + 0.00

MODELING OF LAMINAR COMBUSTION WAVE PROPAGATION IN REACTIVE GAS/PARTICLE MIXTURES

T. LUDWIG and P. ROTH†

Institut für Verbrennung und Gasdynamik, Gerhard-Mercator-Universität, 47048 Duisburg, Germany

(Received 22 December 1995; in revised form 22 August 1996)

Abstract—The ignition and deflagration wave propagation in an enclosed stoichiometric H_2/O_2 mixture enriched with a low mass fraction of carbonaceous particles ignited via a temperature non-uniformity is studied using a one-dimensional numerical model. Different particle diameters, volume fractions, and reactivities are used to investigate their effects on the combustion waves. Detailed chemical kinetics for H_2/O_2 are applied for the gas phase. Particle phase reactions are calculated using measured reaction probabilities for heterogeneous carbon reactions. Both phases being modeled as continua, the governing equations are solved using flux-difference-splitting schemes. A dynamically moving adaptive grid is applied in order to resolve reaction zones correctly. Copyright © 1996 Elsevier Science Ltd.

Key Words: reactive gas/particle flow, Eulerian approach, continuous particle phase, flux-difference-splitting (FDS), dynamically adaptive grid, detailed gas phase kinetics, particle kinetics, reaction probabilities

1. INTRODUCTION

While gaseous deflagration and detonation have been studied intensively since the last century, the literature about combustion and detonation phenomena in heterogeneous gas/particle mixtures is relatively sparse, though these systems have a great practical significance e.g. in dust explosion or in diesel combustion. Combustion waves in heterogeneous gas/particle mixtures have been investigated mainly experimentally for special cases, as, e.g. dust explosions by Proust and Veyssière (1988), Austin *et al.* (1993), Peraldi *et al.* (1993), and Lebecki *et al.* (1993). A systematic consideration of modeling of gas/particle reactions was carried out, e.g. by Baer and Nunziato (1986) related to granular materials, and Igra and Ben-Dor (1988) in an extensive study for dusty shock waves. The mathematical structure of two-phase models was studied, eg. by Stuhmiller (1977) or Embid and Baer (1992). Other authors treat accurately aspects like the modeling of heat radiation or the mass and energy transfer inside a porous particle. The models used for the gas and particle reactions kinetics and for the conservation equations are comparatively simple, see for example Krazinski *et al.* (1979), Sichel (1991), Smirnov (1988), Smirnov and Tyurnikov (1994), Khasainov and Veyssière (1994), or Ha and Choi (1994). Nearly all of these numerical investigations deal with stationary phenomena. Sirignano (1993) gives a comprehensive overview of different modeling approaches for gas/particles mixtures. He directs his attention mainly to the fluid dynamics of sprays and the related vaporisation processes. Krishenik *et al.* (1994) model accurately the heat transfer between the two phases assuming a zero velocity for the mixture of gas and particles and using a one-step model for the chemical reactions. Smirnov (1988) and Smirnov and Tyurnikov (1994) use a non-stationary model for gas/particle flames and detonations in a tube neglecting viscosity and diffusion in the gas phase. Fan and Sichel (1988) consider the modeling of the heterogeneous reactions but treat gas and particles together as a single fluid in the framework of stationary conservation equations.

From the point of view of modeling heterogeneous combustion, mainly two ways may be distinguished. On the one hand, in the so-called Lagrangian approach, the particles are treated each for its own, whereas on the other hand in the so-called Eulerian approach the particles are assumed to be equally distributed so that gas and particles may be treated as two interacting continua. The Lagrangian approach is often used for large particles (see Tsuji *et al.* 1989). In the work of Baer and Nunziato (1986), e.g. gas and particles are treated as continua for porous reactive materials.

†Author to whom correspondence should be addressed.

Smirnov (1988), Smirnov and Tyurnikov (1994), Khasainov and Veyssière (1994), Fan and Sichel (1988), and Hayashi and Fuyuto (1989) use the continuum formulation also for reactive gas/particle flows.

In the present paper, the continuum Eulerian formulation for the particle phase has been chosen, which was found to be more suited for combustion situations with higher particle concentrations and low mass fractions of particles. It is applied to dilute systems with particle volume fraction around $\epsilon_P = 10^{-4}$. The aim of the present paper is to present a model, which includes the conservation equations, the transport properties, the reaction source terms, and the interphase fluxes. The numerical method used for the spatial and temporal solution of the equations is described in detail. In the results section, the influence of different degrees of particle reactivity and particle load on the structure of deflagration and detonation waves is illustrated. As we want to investigate fundamental effects of gas/particle combustion, we use a closed vessel with adiabatic walls as an idealized setup. Therefore, a comparison with results from experiments is not possible.

2. ONE-DIMENSIONAL THEORY FOR REACTIVE TWO-PHASE FLOWS

2.1. Conservation equations

In this study, the influence of reactive particles on combustion phenomena in a reactive gas flow is considered using a one-dimensional model. It consists of the reactive Navier–Stokes equations for the gas phase and the reactive Euler equations for the particle phase, enhanced by models for transport processes and detailed reaction kinetics. In the following equations, all variables subscripted with 'P' belong to the particle phase, the variables subscripted with 'G' belong to the gas phase.

The first step is to define the thermodynamical and fluid-mechanical properties of the two-phase mixture. The partial density ρ_{G_k} of the gas phase species k and the continuum particle density ρ_P are defined as the respective masses per unit volume of mixture:

$$\rho_{G_k} = \frac{m_{G_k}}{V}\,; \quad \rho_P = \frac{m_P}{V} \tag{1}$$

with $V = V_P + V_G$ and $\rho_G = \sum_k \rho_{G_k}$. It is useful to introduce the volume fraction of the particles by

$$\epsilon_P = \frac{V_P}{V}\,. \tag{2}$$

For the gas phase, a mass weighted mean velocity is defined based on the absolute velocities u_{G_k} of the different species k by

$$u_G = \sum_k \frac{\rho_{G_k} u_{G_k}}{\rho_G}\,. \tag{3}$$

The particle velocity u_P is averaged over the finite control volume.

The gas pressure is calculated from the gas density ρ_G, the mass specific gas constant R_G, and the gas temperature T_G according to the ideal gas law:

$$p_G = \rho_G R_G T_G\,. \tag{4}$$

p_G is not the really observable gas pressure because the gas density ρ_G is related not only to the gas volume but to the mixture volume. The really observable gas pressure p_{gas} is higher by a factor of $1/(1 - \epsilon_P)$:

$$p_{gas} = \frac{p_G}{1 - \epsilon_P} = \frac{\rho_G}{1 - \epsilon_P} R_G T_G. \tag{5}$$

The gas phase is assumed to be thermally and calorically ideal. The solid phase is supposed to consist of smooth, spherical, non-interacting, and electrically neutral particles. The particles are supposed to be non-compressible, and their porosity is modeled via a porosity coefficient κ_P defined below. However the particle density ρ_P is variable because it is related to the volume of suspension, and not to the particle volume. The temperature inside the particles is assumed to be constant and

equal to their surface temperature. Internal energy and temperature of the particles are related by the equation:

$$E_P = \int_0^{T_P} c_v(T_P)\, dT_P + \tfrac{1}{2}u_P^2,$$

c_v being the heat capacity of the particles depending on the particle temperature. As E_P is the variable in our system, T_P is iterated from the calculated values of E_P and u_P. In the whole system, turbulence effects and volume forces as, e.g. gravity are neglected. The interactions between the particle phase and the gas phase are modeled by interphase flux terms for mass, momentum, and energy. The whole system is considered to be adiabatic.

The governing equations for reactive gas/particle flows consist of the conservation equations for mass, momentum, and energy of both phases, and a convective transport equation for the particle number density. In flux vector form, this system of partial differential equations can be formally written as

$$\mathbf{u}_t + \mathbf{F}_x = \mathbf{Q}, \qquad [6]$$

with **u**, **F**, and **Q** as the vector of the conservative variables, the flux vector, and the vector of source and interphase flux terms, respectively. The subscripts t and x denote derivatives to time and to space.

The vector **u** of the conservative variables is composed of species densities, momentum, and energy of gas and particle phase as well as the particle number density n_P:

$$\mathbf{u} = (\rho_{G_k} \quad \rho_G u_G \quad \rho_G E_G \quad \rho_P \quad \rho_P u_P \quad \rho_P E_P \quad n_P)^T. \qquad [7]$$

E_G and E_P are the total energies of the gas and the particle phases per unit mass.

The flux vector **F** can be divided into the vector of the convective flux $\mathbf{F}_{con}$ and the vector of the viscous and diffusive fluxes $\mathbf{F}_{vd}$:

$$\mathbf{F} = \mathbf{F}_{con} + \mathbf{F}_{vd}. \qquad [8]$$

The convective flux vector $\mathbf{F}_{con}$ also contains momentum and energy fluxes due to pressure gradients. The viscous/diffusive flux vector $\mathbf{F}_{vd}$ is composed of the diffusional mass fluxes j_k of the gaseous species k relative to the mean gas velocity u_G, the energy diffusion flux j_q, and the viscous momentum and energy fluxes of the gas phase

$$\mathbf{F}_{con} = \begin{bmatrix} \rho_{Gk} u_G \\ \rho_G u_G^2 + (1-\epsilon_P) p_{gas} \\ \rho_G E_G u_G + (1-\epsilon_P) p_{gas} u_G \\ \rho_P u_P \\ \rho_P u_P^2 + \epsilon_P p_{gas} \\ \rho_P E_P u_P + \epsilon_P p_{gas} u_P \\ u_P n_P \end{bmatrix} \quad \mathbf{F}_{vd} = \begin{bmatrix} j_k \\ -\frac{4}{3}\mu \dfrac{\partial u_G}{\partial x} \\ -\frac{4}{3}\mu \dfrac{\partial u_G}{\partial x} u_G + j_q \\ 0 \\ 0 \\ 0 \\ 0 \end{bmatrix}. \qquad [9]$$

The source term vector **Q** contains both the chemical source terms $\dot{\omega}_k$ and the interphase fluxes J, f, and q, which can be considered as source terms for each phase:

$$\mathbf{Q} = \begin{bmatrix} \dot{\omega}_k \\ J u_P + f \\ J E_P + f u_P + q \\ -J \\ -J u_P - f \\ -J E_P - f u_P - q \\ 0 \end{bmatrix}. \qquad [10]$$

The interphase flux term JE_P corresponds to the energy, which is transfered to the gas phase from the disappearing solid particles. Two limiting cases can be considered:

(1) The energy JE_P is totally added to the gas phase, thus increasing the gas temperature in case of an exothermic reaction.
(2) The energy JE_P is totally added to the solid phase causing a particle heat-up in case of an exothermic reaction. For this case, the sign before JE_P in the equations for the conservation of energy of the gas and the particle phase has to be inversed.

In the above equations, the first case is implemented. For the second case, only the sign of the term JE_P in the energy equations of gas and particles has to be inversed. The total mixture relations are therefore not influenced. For the examples presented here, both limiting cases have been tested. Except for slight differences in the absolute temperatures of gas and particles, visible differences could not be stated.

The formulation of the governing equations is coherent so that the mixture conservation equations arise when adding the corresponding conservation equations of the two phases.

2.1.1. The particle pressure problem. The flux term $\epsilon_P p_{gas}$ in $\mathbf{F}_{con}$ can, at first glance, be interpreted as a particle pressure. In fact, our model does not permit collisions between the particles and hence pressure forces due to the particles are not allowed. Differentiating the above-cited pressure flux term $\epsilon_P p_{gas}$ to the spatial variable x we receive:

$$\frac{\partial}{\partial x}(\epsilon_P p_{gas}) = \epsilon_P \frac{\partial}{\partial x} p_{gas} + p_{gas} \frac{\partial}{\partial x} \epsilon_P. \qquad [11]$$

The first term on the right side represents the force that a gradient in the gas phase pressure exerts on the particles due to different pressure forces at the different sides of the particles like it is known from the buoyancy forces. The second term would initiate a temporal change in the particle and gas momentums if a gradient in the particle concentration occurs. This is not intended to be included in our model, so, in order to neutralize this effect, the term $p_{gas}\partial\epsilon_P/\partial x$ is also included in the momentum flux f in the source term vector $\mathbf{Q}$, as it is described later. It is not directly subtracted from or added to the flux terms in order to maintain the flux-vector form of the equation system convenient for the application of flux-difference splitting schemes. The corresponding term in the energy equations is treated in a similar way.

Concerning the mathematical character of the system of differential equations it is known that the Euler equations for the gas and particle phase are hyperbolic, except for some special cases, where it degenerates to a parabolic system (Gonthier and Powers 1995). The addition of viscous, diffusive, and conductive terms to the gas phase equations (⇒Navier–Stokes equations) alters the character to parabolic type, whereas the pressure correction term does not have such an effect. Nevertheless, the flux-difference splitting scheme used is only applied to the Eulerian part of the system, which is in general hyperbolic, whereas the viscous, diffusive, and conductive terms and the pressure correction were central differenced and treated as source terms.

2.2. Viscous/diffusive fluxes

2.2.1. Viscous fluxes. For the viscous momentum and energy fluxes, the gas phase is supposed to have the properties of a Newtonian fluid. The viscous fluxes are modeled as $\frac{4}{3}\mu\,\partial u_G/\partial x$ and $-\frac{4}{3}\mu u_G\,\partial u_G/\partial x$ as given in $\mathbf{F}_{vd}$. The viscosity μ is considered mixture averaged. It is taken from a computer code package for multicomponent transport properties by Kee *et al.* (1983), where it is determined from a semi-empirical formula by Wilke (1950).

2.2.2. Species diffusion j_k. The diffusion term j_k is modeled as

$$j_k = \rho_G Y_{G_k} v_{G_k}. \qquad [12]$$

The mass fraction Y_{G_k} is the ratio of the density of gas phase species k to the total gas density ρ_G. The diffusion velocity v_{G_k} is defined as the velocity of a species relative to the mean gas velocity. Following Kee *et al.* (1983) it contains:

- diffusion due to gradients in concentration (v_{Dk}), [14]
- thermo-diffusional effects (v_{Tk}), [15]
- a correction term due to the inaccuracy in modeling the two above effects (v_c).

For a species k they define:

$$Y_{G_k} v_{G_k} = Y_{G_k} v_{D_k} + Y_{G_k} v_{T_k} + Y_{G_k} v_c. \quad [13]$$

Approaches to these terms are given by the Fickian formulae:

$$Y_{G_k} v_{D_k} = -D_k \frac{M_k}{\bar{M}} \frac{dX_{G_k}}{dx} \quad [14]$$

$$Y_{G_k} v_{T_k} = \frac{M_k}{\bar{M}} D_k \Theta_k \frac{1}{T_G} \frac{dT_G}{dx}. \quad [15]$$

In [14] and [15], X_{G_k} is the molar fraction of component k, Y_{G_k} the corresponding mass fraction. $\bar{M}$ and M_k are the molar weights of the mixture and of species k. Θ_k is the ratio between thermal and molecular diffusion (due to gradients in concentration) of component k. D_k is the diffusion coefficient of species k into the mixture. It can be calculated from

$$D_k = \frac{\sum_{i \neq k}^{N_{gas}} (X_{G_i} M_i)}{\bar{M} \sum_{i \neq k}^{N_{gas}} (X_{G_i} / D_{ki})}, \quad [16]$$

where D_{ki} is the binary diffusion coefficient of species k into species i.

In the approach by Kee *et al.* (1983), which based upon the work of Coffee and Heimerl (1981), a correction term was introduced for the diffusion velocity guaranteeing that the mass weighted sum over the species velocities gives the mean gas velocity u_G:

$$\sum_{k=1}^{N_{gas}} [Y_{G_k} (u_G + v_{G_k})] = u_G. \quad [17]$$

This is equivalent to a vanishing sum of the mass weighted diffusion velocities:

$$\sum_{k=1}^{N_{gas}} (Y_{G_k} v_{G_k}) = 0. \quad [18]$$

The correction term u_c can then be calculated from

$$Y_{G_k} v_c = -Y_{G_k} \sum_{i=1}^{N_{gas}} (Y_i v_{D_i} + Y_i v_{T_i}). \quad [19]$$

2.2.3. Energy diffusion j_q. In our model the energy diffusion contains the thermal conductivity inside the gas and the energy transport due to the species flow. The energy diffusion j_q can be modeled by

$$j_q = -\lambda \frac{\partial T_G}{\partial x} + \rho_G \sum_{k=1}^{N_{gas}} (h_k Y_{G_k} v_{G_k}), \quad [20]$$

h_k being the mass related enthalpy of component k and λ the thermal conductivity of the gas mixture calculated based on a combination averaging formula of the pure species conductivities by Mathur *et al.* (1967):

$$\lambda = \frac{1}{2} \left[\sum_{k=1}^{N_{gas}} X_k \lambda_k + \frac{1}{\sum_{k=1}^{N_{gas}} X_k \lambda_k} \right]. \quad [21]$$

The pure species conductivities were assumed to be composed of the translational, rotational, and vibrational contributions as given by Warnatz (1982).

2.3. Chemical source terms

The source terms $\dot{\omega}_k$ ($k = 1, \ldots, N_{\text{gas}}, P$) for all gas phase species and the dispersed solid phase are calculated from both the detailed gas phase kinetics of the homogeneous reactions and the global heterogeneous reactions. The total mechanism of homogeneous and heterogeneous reactions can be formally written as

$$\sum_{k=1}^{N_{\text{gas}}} \nu_{k,j} G_k + \mu_j P \overset{j,-j}{\rightleftharpoons} \sum_{k=1}^{N_{\text{gas}}} \nu_{k,-j} G_k, \quad j = 1 \ldots N_{\text{hom}} + N_{\text{het}}. \tag{22}$$

G_k are the gaseous species, $\nu_{k,j}$ and $\nu_{k,-j}$ are their stoichiometric coefficients. P represents the particle species, μ_j its stoichiometric coefficient. N_{gas} is the number of gaseous species in the reaction mechanism. j and $-j$ represent the forward and backward channels of the reactions. For simplification reasons, the heterogeneous gas/particle reactions are arranged in the total mechanism after the homogeneous gas phase reactions. This implicates $\mu_j = 0$ for $j \leqslant N_{\text{hom}}$ and $\mu_j \neq 0$ for $j > N_{\text{hom}}$. For each heterogeneous reaction, it is assumed that only one gas phase species reacts with the solid particle, so that for a fixed $j > N_{\text{hom}}$ only one $\nu_{k,j}$ is different from zero. The source terms $\dot{\omega}_k$ for the gas phase species k due to homogeneous and heterogeneous reactions can be calculated from

$$\dot{\omega}_k = M_k \sum_{j=1}^{N_{\text{hom}}+N_{\text{het}}} -(\nu_{k,j} - \nu_{k,-j})\dot{r}_j, \quad k = 1 \ldots N_{\text{gas}}$$

with M_k being the molar mass of species k. Different methods for representing the reaction rates r_j will be used for the homogeneous and heterogeneous reactions:

$$\dot{r}_j = R_j \text{ for the homogeneous reactions } (j \leqslant N_{\text{hom}})$$

$$\dot{r}_j = S_j \text{ for the heterogeneous reactions } (j > N_{\text{hom}}).$$

2.3.1. Homogeneous reactions. The homogeneous reaction rate R_j of an elementary reaction j is calculated from the rate coefficients k_j and k_{-j} of the forward and backward reactions, the species densities ρ_k, and the molar masses M_k:

$$R_j = k_j \prod_{k=1}^{N_{\text{gas}}} \left(\frac{\rho_{G_k}}{M_k}\right)^{\nu_{k,j}} - k_{-j} \prod_{k=1}^{N_{\text{gas}}} \left(\frac{\rho_{G_k}}{M_k}\right)^{\nu_{k,-j}}, \quad j = 1 \ldots N_{\text{hom}}. \tag{23}$$

The rate coefficient k_j depends on the gas temperature and can be represented by an Arrhenius expression:

$$k_j(T_G) = A_j T_G^{n_j} \exp\left(-\frac{T_{a_j}}{T_G}\right). \tag{24}$$

A_j is the frequency factor, n_j the temperature exponent, and T_{a_j} the activation temperature of reaction j. For many elementary reactions the temperature exponent n_j vanishes, so that the logarithm of the rate coefficient $\ln k_j$ is a straight line over reciprocal temperature $1/T_G$. In general, the rate coefficient of an elementary reaction has to be determined in kinetic experiments, theoretical calculations are not satisfactory up to now. The backward rate coefficient $k_{-j} = k_j/K_{cj}$ of an elementary reaction j is calculated from the forward rate coefficient of k_j and the equilibrium constant K_{cj}, which can be determined from the thermodynamical data.

2.3.2. Heterogeneous reactions. The heterogeneous reaction rate S_j, which is defined by the rate of change of the dispersed solid material due to the heterogeneous reaction j, can be calculated from

$$S_j = \frac{1}{\left(\sum_{k=1}^{N_{\text{gas}}} \nu_{k,j}\right)^2} \alpha_j a_P \sum_{k=1}^{N_{\text{gas}}} \nu_{k,j} Z_k, \quad j = N_{\text{hom}} + 1 \ldots N_{\text{hom}} + N_{\text{het}}. \tag{25}$$

The properties μ_j, α_j, a_P, $\nu_{k,j}$, and Z_k in the above equation are the stoichiometric coefficient of the solid species, the reaction probability, the particle surface per unit volume of suspension, the stoichiometric coefficient of the gaseous species reacting with the solid species, and the number of collisions of the reacting gas phase species k with the particles per unit time and unit particle surface. As in the case of homogeneous reactions, the reaction probability α_j for the heterogeneous reactions can be represented by an Arrhenius expression:

$$\alpha_j = A_j \exp\left(-\frac{T_{a_j}}{T_P}\right) \qquad [26]$$

with T_P being the particle surface temperature. α_j, that lies between 0 and 1, describes the number of reactive collisions of species j with the particle surface compared to the total number of collisions.

For spherical particles of monodisperse size, the specific particle surface a_P can be calculated from the particle diameter D_P, the particle number density n_P, and the particle porosity κ_P. The last mentioned property is the ratio of the real reactive surface of the particle to the surface of a smooth sphere. The particle diameter D_P can be calculated from the particle mass and number densities ρ_P and n_P

$$a_P = \pi D_P^2 n_P \kappa_P. \qquad [27]$$

The collision number Z_k is determined from the Hertz–Knudsen equation:

$$Z_k = \frac{1}{4}\frac{\rho_{G_k}}{M_k}\sqrt{\frac{8}{\pi}R_k T_G} \qquad [28]$$

with k being the index of the gas phase species k. The properties ρ_{G_k}, M_k, R_k, and T_G are its density, molar mass, gas constant, and the gas temperature, respectively. Strictly speaking, this equation is only valid if gas and particles have the same velocity. Heterogeneous reactions mainly take place when the particles have achieved their ignition temperature by convective heat transfer. At this moment, particle and gas velocities are nearly the same.

2.4. *Interphase fluxes*

2.4.1. Mass flux J. The mass exchange J between the gas phase and the particle phase due to heterogeneous reactions is equal to the sum of the production rates of the gaseous species $\dot{\omega}_k$ ($k = 1 \ldots N_{gas}$) or to the consumption rate of the solid species P:

$$J = \sum_{k=1}^{N_{gas}} \dot{\omega}_k = -\dot{\omega}_P. \qquad [29]$$

2.4.2. Momentum flux f. The interaction forces between the gas phase and the particle phase are represented by the drag force:

$$f_{drag} = \tfrac{1}{2} c_D \rho_G (u_P - u_G)|u_P - u_G| \pi D_P^2 n_P, \qquad [30]$$

where D_P is the diameter of a particle, n_P the number of particles per unit volume and c_D the drag coefficient of a sphere, which depends on the Reynolds number

$$\mathrm{Re} = \frac{|u_G - u_P| D_P}{\nu} \qquad [31]$$

with ν being the kinematic viscosity of the gas. Although the flow around the particles is unsteady, the following formulas for the drag coefficients for stationary flows were used:

$$0 < \mathrm{Re} \leqslant 0.2 \quad c_D = 24/\mathrm{Re} \quad \text{(Stokes)}$$
$$0.2 < \mathrm{Re} \leqslant 1 \quad c_D = 27/\mathrm{Re}^{0.84} \quad \text{(in Boothroyd 1971)}$$
$$1 < \mathrm{Re} \leqslant 1000 \quad c_D = 24/\mathrm{Re} \times (1 + 0.15\mathrm{Re}^{0.687}) \quad \text{(Boothroyd 1971)}$$

For Knudsen numbers $\mathrm{Kn} = l/D_P$ (l is the mean free path of the gas molecules) around 1 or larger, the continuum expression for the drag coefficient c_D must be modified due to molecular effects, see Friedlander (1977):

$$c_{D_c} = c_D(1 + 2\mathrm{Kn}A)^{-2}. \qquad [32]$$

The factor A in this equation is:

$$A = 1.257 - 0.4 \exp\left(\frac{-0.55}{\mathrm{Kn}}\right). \quad [33]$$

According to Fuchs (1964), the Basset force was neglected in particle/gas flows because the ratio of the densities of particles and gas is large. Combustion effects on the drag force were not considered.

As stated in the section dealing with the particle pressure problem, the term $p_{\mathrm{gas}}\partial\epsilon_{\mathrm{P}}/\partial x$ is added to the momentum flux:

$$f = f_{\mathrm{drag}} - p_{\mathrm{gas}}\frac{\partial\epsilon_{\mathrm{P}}}{\partial x}$$

2.4.3. Energy flux q. The relevant mechanisms for the heat transfer between gas and particle phase are the convective and the radiative fluxes. Here only the convective heat transfer has been regarded, whereas the radiative transfer is planned for a later stage. The convective heat transfer is modeled by

$$q_{\mathrm{convective}} = \lambda \mathrm{Nu} \pi D_{\mathrm{P}} (T_{\mathrm{P}} - T_{\mathrm{G}}) n_{\mathrm{P}}. \quad [34]$$

The Nusselt number $\mathrm{Nu} = \alpha/D_{\mathrm{P}}/\lambda$ contains the heat transfer coefficient α and the heat conductivity λ of the ambient gas. In the case of only heat conduction, the Nusselt number is equal to $\mathrm{Nu} = 2$. For spherical particles, the Nusselt number can be calculated from the Reynolds and Prandtl numbers:

$$\mathrm{Nu} = 2 + 0.7\mathrm{Re}^{1/2}\mathrm{Pr}^{1/3}. \quad [35]$$

Combustion effects on the convective heat transfer have been neglected. Re and Pr are defined as usual.

3. NUMERICAL METHOD

The temporal and spatial stiffnesses of the system of differential equations describing reactive flows, which are caused by steep gradients in space and which have very different time scales for the reactions, require a special numerical treatment. To receive correct results in the simulations, it is essential to follow the formation and consumption of radicals inside a flame by using a computational grid with arbitrary cell widths in the physical domain. A special algorithm formulated as differential equation for each cell determines the cell widths corresponding to the desired resolution of the important zones. The resulting system of differential equations is spatially discretized using the method of lines. The temporal part is solved implicitly using the solver package DASSL (see Petzold 1983).

3.1. Spatial discretisation

The first step for the spatial discretisation is to put a numerical spatial grid on the given physical problem. In this study, arbitrary spaced grids have been applied. For each grid point, a set of conservation equations like [6] can be written in the form

$$\mathbf{u}_t + \mathbf{F}'_x = \mathbf{Q}', \quad [36]$$

where the indices t and x indicate derivatives to time and to space. $\mathbf{u}$ is the vector of the conservative variables and $\mathbf{F}'$ the flux vector. $\mathbf{Q}'$ is the source term vector. For numerical reasons $\mathbf{F}'$ contains only the convective flux $\mathbf{F}_{\mathrm{con}}$ from [9] whereas $\mathbf{Q}'$ equals to $\mathbf{F}_{\mathrm{vd}_x} + \mathbf{Q}$ from [9] and [10].

Various methods are known to calculate the fluxes. As the flame code should also allow to investigate the transition from deflagration to detonation, some expense is put on the treatment of shocks and contact discontinuities. There are several possibilities, e.g.

- Front tracking: the cell boundaries are moved with the discontinuities. Therefore a shock detection condition has to be defined.
- Shock fitting: the calculations are only performed in non-shock regions. The shocks themselves are treated separately by the Rankine–Hugoniot relations for shocks; discontinuities have also to be detected.

- Shock capturing: the whole computational domain is treated by one numerical method. It includes a conservative formulation of the governing equations and takes care of the Rankine–Hugoniot conditions.

In this study the flux-difference-splitting (FDS) method is applied that belongs to the family of shock capturing schemes. FDS methods are approximate Riemann solvers assuming a wave propagation from each cell boundary. The main idea is to split the fluxes according to their domains of influence. In this work, the convective gas phase fluxes (F_{con} in [9]), i.e. the hyperbolic part of the system, are treated by a second order upwind flux-difference-splitting (FDS) scheme by Harten and Yee (see Yee 1987) that gives very precise results for shocks and contact discontinuities. The viscous–diffusive fluxes $\mathbf{F}_{vd}$ are treated as source terms. Liu and Vinokur (1989) give an overview how to apply upwind algorithms to chemically reacting flows even if they are not in equilibrium. The particle phase fluxes are calculated by an upwind FDS scheme introduced by Harten *et al.* (1983). It has been chosen because of its simplicity. A more detailed FDS scheme is not necessary because the particles are only influenced by their direction of propagation.

3.2. Moving adaptive grid

The moving adaptive grid (see Dorfi and Drury 1987; Mack *et al.* 1991) has been used to reduce the number of mesh points allowing nevertheless a good resolution in zones where more points are needed. Flame zones, for example, need a good resolution, so that the real reaction kinetics in flames can be simulated. The criterion for the method applied here is to equi-distribute the arc-lengths of a special monitor function, which is combination of the slopes of the variables used in the problem, over the spatial coordinate. In a simple case, the monitor function is taken to be equal to the gas temperature. The cell boundaries will move allowing the arc-length of temperature over the spatial coordinate to be the same in all cells. Figure 1 illustrates the principle and shows that in regions with steep gradients the cell widths decrease.

The monitor function in cell i is defined as

$$M_i = \sqrt{1 + \sum_j c_j \left(\frac{u_{j,i+1/2} - u_{j,i-1/2}}{x_{i+1/2} - x_{i-1/2}} \right)^2}, \qquad [37]$$

where $u_{j,i+1/2}$ is a variable (e.g. temperature, pressure, etc.) at the right boundary of cell i and c_j a weighting coefficient for the corresponding variable. $x_{i+1/2}$ is the position of the right boundary

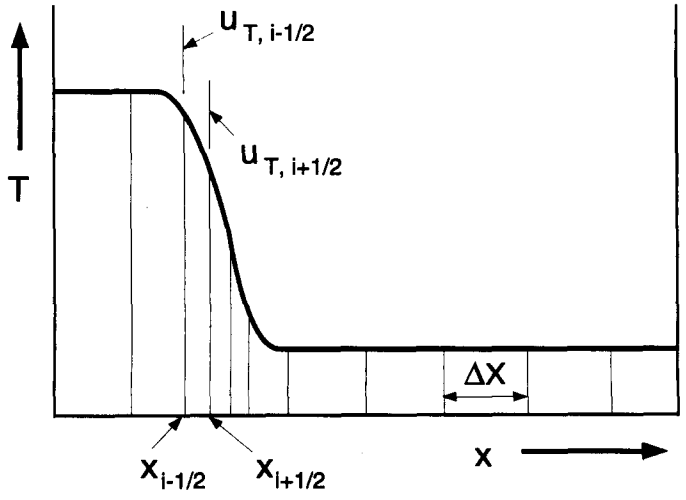

Figure 1. Example for the arc-length equi-distribution principle using a temperature profile: in each cell the arc-length is the same so that in regions with steep gradients the cell widths are small.

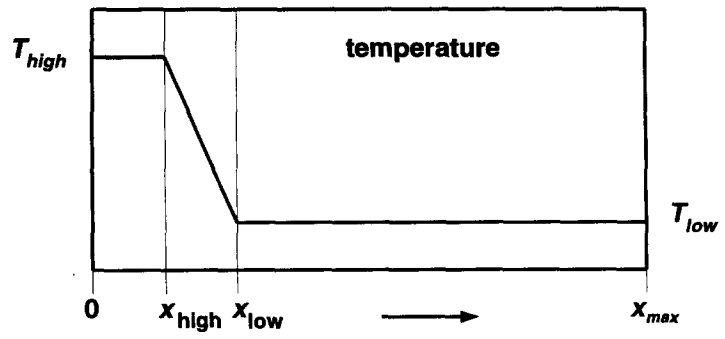

Figure 2. Initial temperature profile of the closed vessel flame problem.

of cell i. This monitor function multiplied by the cell width has to be constant over the whole computational domain. This condition is formulated recursively:

$$\Delta x_i M_i - \Delta x_{i-1} M_{i-1} = 0. \qquad [38]$$

Due to stability reasons, the movement of the cell boundaries is damped in the following way:

$$0 = \tau_g \left(\frac{dx_i}{dt} M_i - \frac{dx_{i-1}}{dt} M_{i-1} \right) + \Delta x_i M_i - \Delta x_{i-1} M_{i-1}, \qquad [39]$$

where τ_g is a time constant for the grid movement. Moreover, a distortion limitation has been introduced so that the ratio of the cell widths of neighbored cells is held between given limits. The grid equations result in one additional differential equation per cell. They are solved together with the conservation equations for each cell.

3.3. Temporal solution

The temporal solution of the spatially discretized system of differential equations cannot be made explicitly because of the very stiff character of this system due to very large differences in the time scales of both the detailed chemical reaction and the gas/particle flow. Therefore the implicit solver DASSL (see Petzold 1983) has been used for the conservation equations as well as for the grid equations. DASSL is based upon Gear methods and is able to solve differential equation systems of the form $0 = \mathbf{g}(t, \mathbf{y}, d\mathbf{y}/dt)$.

4. RESULTS: INFLUENCE OF PARTICLES ON COMBUSTION WAVES

4.1. Initial and boundary conditions

4.1.1. Initial conditions. The calculations were performed for an enclosed H_2/O_2 mixture at an initially uniform pressure enriched with particles choosing another degree of reactivity, diameter, and concentration for each calculation. The initial temperature profile used is shown schematically in figure 2. From a small high temperature region (T_{high}) at the left side, the temperature decreases linearly between x_{high} and x_{low} to a low temperature region (T_{low}). The initial data for the confined gas/particle mixture are:

- gas phase pressure $p^0 = 1$ bar,
- $x_{high} = 0.2$ cm, $x_{low} = 0.3$ cm, $x_{max} = 3$ cm,
- temperature levels $T_{high} = 1100$ K, $T_{low} = 800$ K,
- stoichiometric H_2/O_2 mixture,
- particle diameter $D_P^0 = 0.369\ \mu$m, $3.69\ \mu$m, or $36.9\ \mu$m, particle porosity $\kappa_P = 1$,
- particle volume fraction $\epsilon_P{}^0 = 7.9 \times 10^{-5}$.

The H_2/O_2 mechanism including two CO reactions contains 20 elementary homogeneous reactions of 10 gas phase species (H_2, O_2, O, H, OH, HO_2, H_2O, H_2O_2, CO, CO_2) and is completed by three

Table 1. Homogeneous reaction mechanism and rate coefficient data, $k_j = A_j \times T^{n_j} \times \exp(-T_{a_j}/T)$. The basic units for A_j are cm, s, and moles

No.	Reaction	A	n	T_a[K]	Reference
1	$H + O_2 \rightleftharpoons OH + O$	2.0×10^{14}	0	8449	Baulch *et al.* (1992)
2	$O + H_2 \rightleftharpoons OH + H$	1.5×10^{7}	2.0	3798	Warnatz (1984)
3	$OH + H_2 \rightleftharpoons H_2O + H$	1.0×10^{8}	1.6	1658	Warnatz (1984)
4	$2OH \rightleftharpoons H_2O + O$	1.5×10^{9}	1.14	0	Ernst *et al.* (1977)
5	$2H + M \rightleftharpoons H_2 + M$	9.7×10^{16}	−0.6	0	Warnatz (1984)
6	$H + OH + M \rightleftharpoons H_2O + M$	2.2×10^{22}	−2.0	0	Tsang and Hampson (1986)
7	$H + O_2 + M \rightleftharpoons HO_2 + M$	2.0×10^{18}	−0.8	0	Warnatz (1984)
8	$H + HO_2 \rightleftharpoons 2OH$	1.5×10^{14}	0	504	Warnatz (1984)
9	$H + HO_2 \rightleftharpoons H_2 + O_2$	2.5×10^{13}	0	348	Warnatz (1984)
10	$O + HO_2 \rightleftharpoons OH + O_2$	2.0×10^{13}	0	0	Warnatz (1984)
11	$OH + HO_2 \rightleftharpoons H_2O + O_2$	2.0×10^{13}	0	0	Warnatz (1984)
12	$2HO_2 \rightleftharpoons H_2O_2 + O_2$	8.5×10^{12}	0	504	Warnatz (1977)
13	$2OH + M \rightleftharpoons H_2O_2 + M$	3.2×10^{22}	−2.0	0	Warnatz (1983)
14	$H + H_2O_2 \rightleftharpoons H_2 + HO_2$	1.7×10^{12}	0	1887	Baulch *et al.* (1992)
15	$H + H_2O_2 \rightleftharpoons H_2O + OH$	1.0×10^{13}	0	1803	Warnatz (1984)
16	$O + H_2O_2 \rightleftharpoons OH + HO_2$	2.8×10^{13}	0	3221	Warnatz (1984)
17	$OH + H_2O_2 \rightleftharpoons H_2O + HO_2$	1.0×10^{13}	0	901	Baulch *et al.* (1972)
18	$H_2 + O_2 \rightleftharpoons 2OH$	2.1×10^{14}	0	28979	Estimated
19	$CO + OH \rightleftharpoons CO_2 + H$	4.0×10^{12}	0	4040	Gardiner *et al.* (1973)
20	$CO + O + M \rightleftharpoons CO_2 + M$	5.3×10^{13}	0	−2285	Warnatz (1984)

global heterogeneous reactions. The homogeneous and heterogeneous reactions are shown and referenced in tables 1 and 2.

4.1.2. Boundary conditions. The problem considered is a confined H_2O_2 mixture enriched with carbonaceous particles so that no mass transport across the walls is possible ($u_G = 0$ and $u_P = 0$). Moreover, the walls are assumed to be adiabatic so that also no energy transport across the walls is possible. Consequently the flux vector at the walls is set to

$$\mathbf{F}_{\text{wall}} = \mathbf{F}_{\text{con}} + \mathbf{F}_{\text{vd}} = \begin{bmatrix} 0 \\ (1-\epsilon_P)p_{\text{gas}} - \frac{4}{3}\mu u_{G_x} \\ 0 \\ 0 \\ \epsilon_P p_{\text{gas}} \\ 0 \end{bmatrix}. \qquad [40]$$

Only a momentum exchange between the wall and the gas/particle flow is possible.

4.2. *Variation of particle diameter and particle concentration*

In this section, the influence of different initial particle diameters on the development of a flame are simulated. In all cases, the initial particle volume fraction has been chosen to be $\epsilon_P{}^0 = 7.9 \times 10^{-5}$. The initial particle diameters for the three cases studied were $D_P = 0.369$, 3.69 and 36.9 μm, which causes a variation on the initial particle concentration of $n_P = 3 \times 10^9$, 3×10^6, and 3×10^3 particles per cm^3. The simulated time is 120 μs so that the ignition phase and the flame propagation can be studied.

As a reference case, the simulation of ignition and flame development in a pure gas mixture was studied first. The left part of figure 3 shows the development of the gas temperature profile. At the right side, the temperature increases rapidly after an ignition delay time of about 35 μs. At the

Table 2. Global heterogeneous reactions and reaction probability data, $\alpha_j = A_j \times \exp(-T_{a_j}/T)$. The basic units for A_j are cm, s, and moles

No.	Reaction	A	T_a [K]	Reference
21	$C_S + O \rightarrow CO$	0.23	0	von Gersum and Roth (1992)
22	$2C_S + O_2 \rightarrow 2CO$	0.1679	10060	von Gersum and Roth (1992)
23	$2C_S + 2OH \rightarrow 2CO + H_2$	0.25	0	Roth *et al.* (1990)

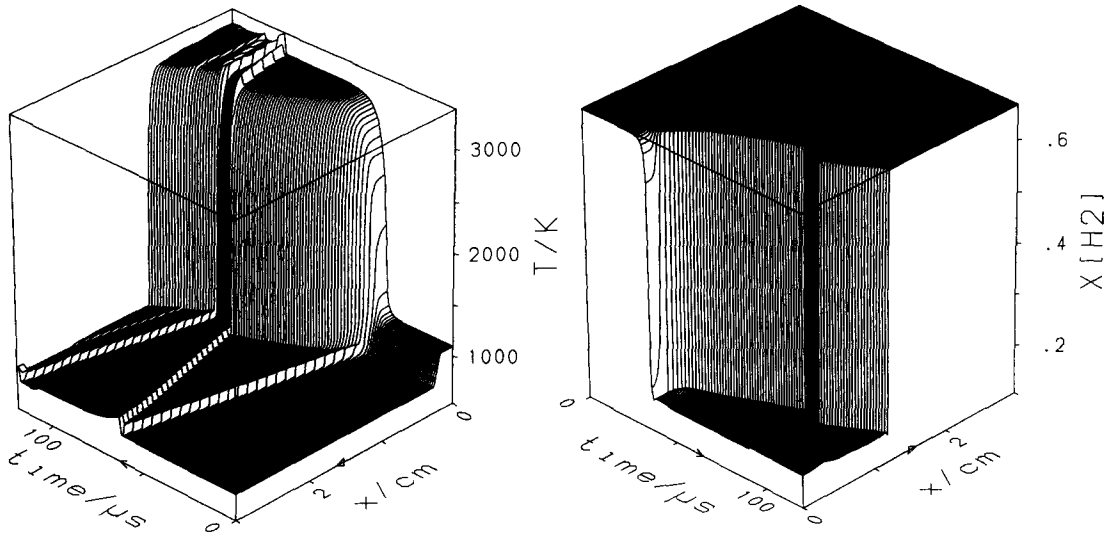

Figure 3. Stoichiometric H_2/O_2 mixture without particles, $p^0 = 1$ bar. Left part: gas temperature, right part: H_2 molar fraction.

time of ignition, a pressure wave starts to propagate with high velocity to the left, which is visible due to the jump in temperature. At the same time, the combustion wave travels to the left but with much lower velocity. The reflected pressure-induced temperature wave meets the flame front and, passing through the burnt gas, it leads to a slight increase in temperature and to a reduction in flame velocity. This is also clearly to be seen in the H_2 molar fraction profile in the right part of figure 3. Note that the orientation of time and space axes is opposite in the left and the right part of figure 3. The steep gradient in the H_2 molar fraction profile marks the position of the flame front. Due to the change in flame velocity, when the reflected pressure wave meets the flame front at about 75 μs, an expansion wave propagates from the flame into the burnt gas and is reflected at the ignition side wall while the compression wave propagates into the unburnt gas and is reflected there, see left part of figure 3.

The simulations with particles revealed that the results for the big particle case ($D_P^0 = 36.9$ μm, $n_P = 3 \times 10^3$ cm^{-3}) are very close to the pure gas phase results. For temperature, pressure, and molar fraction histories, no visible differences appear during the first 120 μs. This is due to the relatively small total particle surface acting for mass, energy, and momentum exchange so that the gas phase properties are only very weakly influenced by the particles. Taking the same particle volume fraction with smaller particles and consequently higher number density, a significant influence of the reacting particles on the calculated results is observed. The left part of figure 4 shows the gas temperature profile history for a mixture with particles with a diameter $D_P = 0.369$ μm and a concentration $n_P = 3 \times 10^9$ cm^{-3}. Compared to the pure gas phase case, ignition takes place at about 38 μs instead of 35 μs. The particle diameter shown in the right part of figure 4 starts decreasing at about the same time and position in the vessel as the gas temperature begins to rise (note the difference in the orientations of time and space axes). Due to the movement of the burnt gas, the particles are not equally distributed so that the particle diameter does not decrease uniformly in the burnt gas region. This effect is more clearly to be seen in the left part of figure 5, where the particle diameter evolution is shown for an initial particle diameter of 3.69 μm. At the burnt gas side, the particle diameter decreases rapidly because this zone is at high temperature from the beginning of the calculations. For times above 80 μs, the particle diameter has a clear local maximum at about 0.7 cm, which is still earlier observable in the particle volume fraction profile in the right part of figure 5. The small difference is due to the burnt gas expansion leading to an acceleration of the particles by the drag forces. So, the particles are accumulated at the initial flame front position and move with their own velocity, which is much lower than the velocity of the flame front located near the local minimum of the particle volume fraction profile. As in the flame front the concentrations of O, OH, and O_2 are much higher than in the burnt gas,

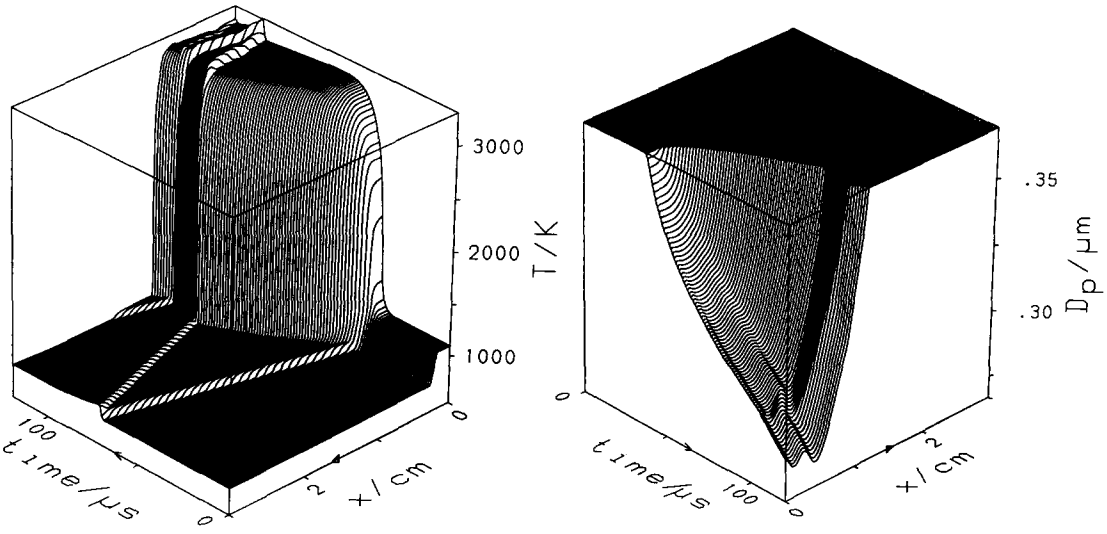

Figure 4. Stoichiometric H_2/O_2 mixture enriched with particles, $p^0 = 1$ bar. Particle properties: $D_P^0 = 0.369$ μm, $\epsilon_P{}^0 = 7.9 \times 10^{-5}$. Left part: gas temperature, right part: particle diameter.

particles are very effectively oxidized there explaining the local minimum in the particle volume fraction, see figure 5, right part. The slight increase of the local maximum in ϵ_P at about 80 μs is due to the reflected ignition-induced pressure wave, which pushes the particles into the burnt gas region. At the unburnt gas side of the vessel, the particles accumulate due to the closed vessel boundary condition.

4.3. Variation of particle volume fraction

The computer simulations in the previous section were performed with an initial particle volume fraction of $\epsilon_P{}^0 = 7.9 \times 10^{-5}$. For the calculations of this section, a value of $\epsilon_P{}^0 = 7.9 \times 10^{-4}$ was chosen which results, for a constant particle diameter $D_P = 3.69$ μm, in a particle concentration of $n_P = 3 \times 10^7$ cm^{-3}, which is by a factor of 10 higher than in the previous case with the same particle diameter. Figure 6 compares the calculated temperature profiles for high and low particle load. The right part representing the case with 10 times more particles reveals that the gas temperature rise is strongly inhibited by the greater amount of particles. The maximum temperature obtained at 100 μs is about 1800 K but reaches in the case with less particles about 3000 K, see

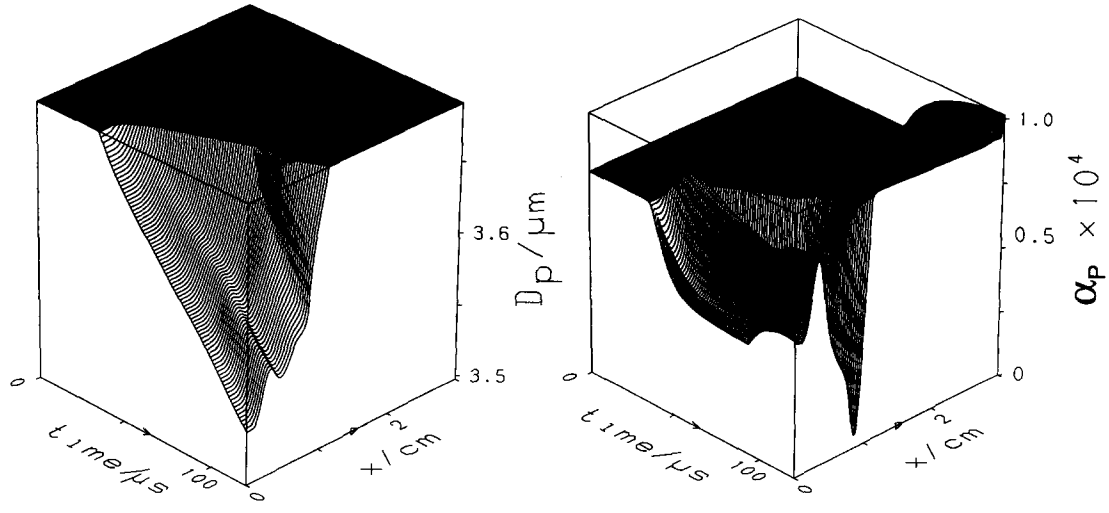

Figure 5. Stoichiometric H_2/O_2 mixture enriched with particles, $p^0 = 1$ bar. Particle properties: $D_P^0 = 3.69$ μm, $\epsilon_P{}^0 = 7.9 \times 10^{-5}$. Left part: particle diameter, right part: particle volume fraction.

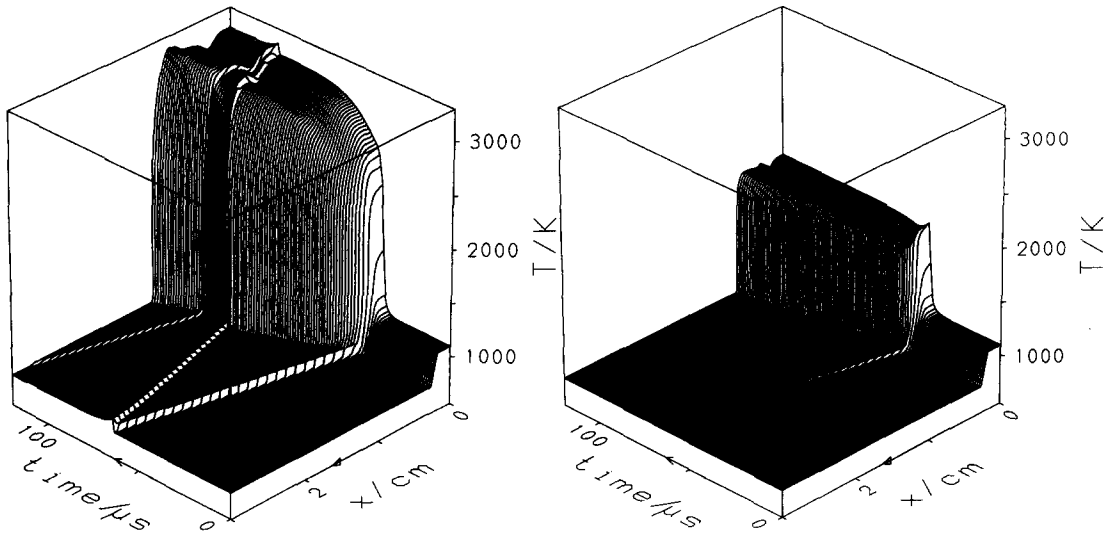

Figure 6. Stoichiometric H_2/O_2 mixture enriched with particles, $p^0 = 1$ bar. Particle properties: $D_P^0 = 3.69\ \mu m$. Left part: gas temperature for $\epsilon_P{}^0 = 7.9 \times 10^{-5}$, right part: gas temperature for $\epsilon_P{}^0 = 7.9 \times 10^{-4}$.

left part of figure 6. The particles partly take the energy released by the gas phase reactions and they also consume radicals by the heterogeneous reactions. It is clearly to be seen that the ignition induced wave is damped out in the case with higher particle load and is nearly invisible shortly after the reflection at the wall. The explanation for the pronounced local minima and maxima in the temperature profile is the same as described in the section before: due to the burnt gas expansion, the particles being initially in the preheating zone of the flame are accumulated in a small region of about 0.1 cm and propagate very slowly to the burnt gas side while the flame front moves faster in the opposite direction. Therefore, the heat loss of the gas is strong in this region and the gas temperature shows a local minimum. As the number of radicals is limited, the particle diameter in figure 7 decreases more slowly in the region of high particle number concentration so that a clear local maximum in the particle diameter evolves.

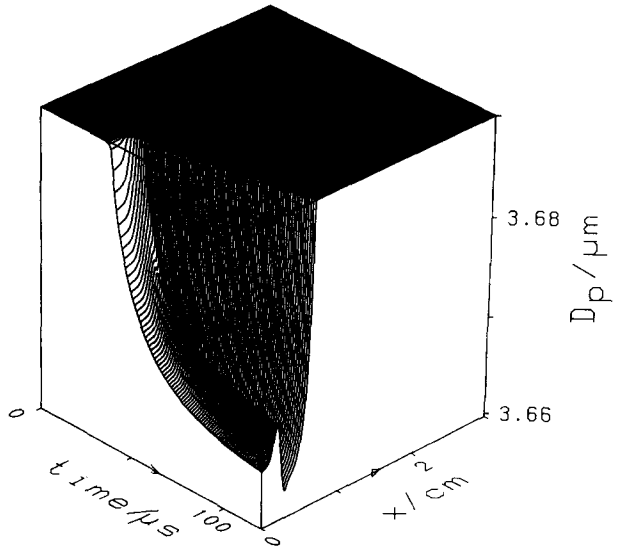

Figure 7. Stoichiometric H_2/O_2 mixture enriched with particles, $p^0 = 1$ bar. Particle properties: $\epsilon_P{}^0 = 7.9 \times 10^{-4}$, $D_P^0 = 3.69\ \mu m$, particle diameter.

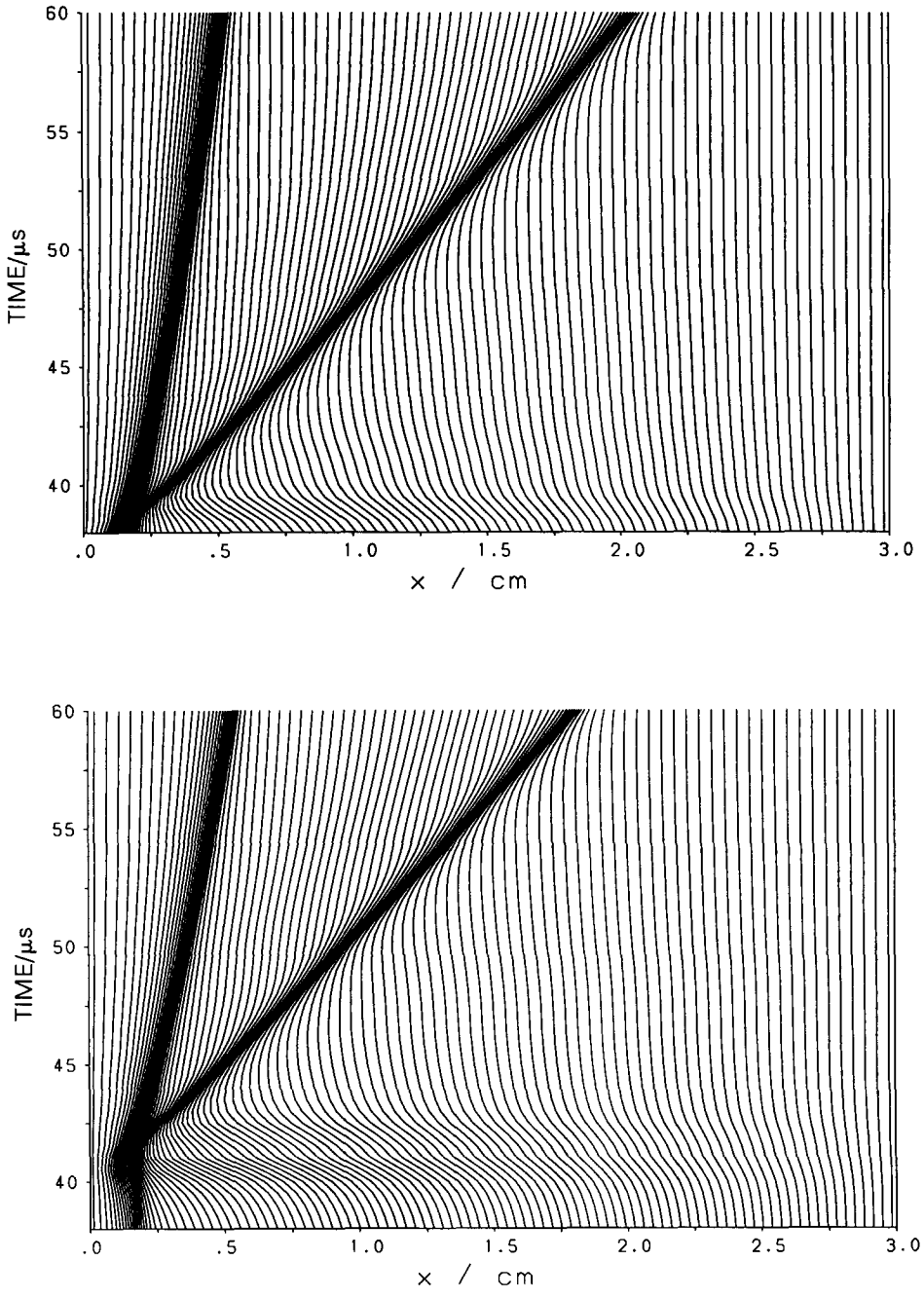

Figure 8. Grid point movement after ignition for a stoichiometric H_2/O_2 mixture enriched with carbonaceous particles. Particle properties: $D_P^0 = 0.369\ \mu m$, $\epsilon_P{}^0 = 7.0 \times 10^{-5}$. Upper part: with measured particle reactivities, lower part: with increased particle reactivities.

4.4. Variation of particle reactivity

For the calculations presented in this section, the particles have a diameter of $D_P = 0.369\ \mu m$ and a concentration of $n_P = 3 \times 10^9\ cm^{-3}$. Two sets of probabilities for the particle reactions are used: measured values according to table 2 and artificially increased reactivities with A-factors equal to $A = 0.9$. In figure 8, the grid point movements after ignition for both cases are shown, upper part normal reactivity, lower part increased reaction probabilities. Each line represents the movement of one cell boundary during the calculation. The stripes of concentrated lines at the left correspond to the flame front, where the gradient of the conserved variables are steep. The other stripes of minor concentrated lines correspond to the ignition-induced pressure waves, the slope

of which is smaller in the case of highly reactive particles indicating a higher propagation velocity. This is due to the larger heat release at the moment of ignition because of the additional energy release of the very strong heterogeneous reactions. The comparison also reveals that for the higher particle reactivity the ignition delay is increased from about 38 to 41 μs. The reason is that the heterogeneous reactions consume O and OH radicals during the pre-ignition phase and hinder in so far the gas phase ignition reactions. However, once ignited, the temperature increase is

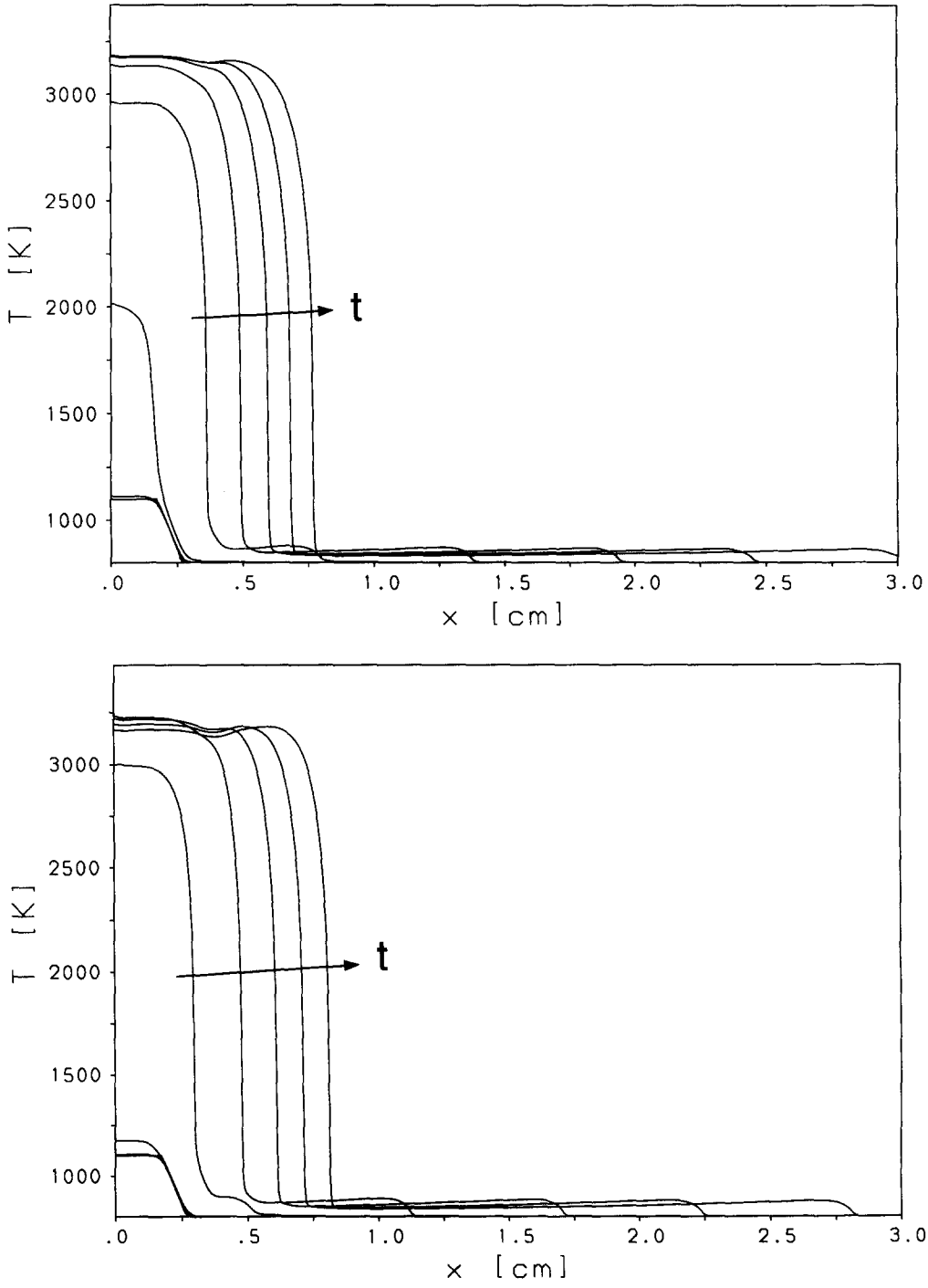

Figure 9. Gas temperature development for a stoichiometric H_2/O_2 mixture enriched with carbonaceous particles. Particle properties: $D_P^0 = 0.369$ μm, $\epsilon_P{}^0 = 7.0 \times 10^{-5}$, $\Delta t = 6.5$ μs, $t_{start} = 0$, $t_{end} = 70$ μs. Upper part: with measured particle reactivities, lower part: with increased particle reactivities.

accelerated by the heterogeneous reactions as shown in figure 9 for the development of the gas temperature. In the highly reactive particle case the gas temperature increases from 1175 to 3000 K during 6.5 μs whereas in the other case this period is only sufficient for an increase from 1150 to 2000 K.

5. CONCLUSION

The present investigation reveals a clear influence of particle diameter and number concentration on the ignition and flame propagation of enclosed H_2/O_2 mixtures enriched with carbonaceous particles. Due to the relatively small active particle surface and the higher particle inertia, the simulations for mixtures with large particles ($D_P^0 = 36.9\ \mu$m, $n_P = 3 \times 10^3$ particles per cm^3) show nearly the same behavior during the first 120 μs of calculation time as mixtures without particles. Smaller particles are strongly influenced by the movement of the gas. Therefore, a local maximum of the particle volume fraction at the initial position of the flame induced temperature ramp grows up. Due to a lack of radicals in the burnt gas region this maximum is not reduced and remains visible up to the end of the simulation period. When increasing the particle volume fraction, the ignition induced wave is damped out and the temperature increase is decelerated. For higher particle reactivities, the ignition induced wave becomes faster and the ignition delay is increased due to the radical consuming heterogeneous reactions.

Acknowledgement—The financial support by the Ministerium für Wissenschaft und Forschung des Landes Nordrhein-Westfalen is gratefully acknowledged.

REFERENCES

Austin, P. J., Kauffman, C. W. and Sichel, M. (1993) Ignition and volatile combustion of cellulosic particles. In *Proceedings of the 14th International Colloquium on the Dynamics of Explosions and Reactive Systems*, Coimbra, Vol. I. Chap. 7.8.

Baer, M. R. and Nunziato, J. W. (1986) A two-phase mixture theory for the deflagration-to-detonation transition (DDT) in reactive granular materials. *Int. J. Multiphase Flow* **12,** 861–889.

Baulch, D. L., Drysdale, D. D., Horne, D. G. and Lloyd, A. C. (1972) *Evaluated Kinetic Data for High Temperature Reactions, Vol. 1: Homogeneous Gas Phase Reactions of the H_2–O_2 system.* Butterworths, London.

Baulch, D. L., Cobos, C. J., Cox, R. A., Esser, C., Frank, P., Just, Th., Kerr, J. A., Pilling, M. J., Troe, J., Walker, R. W. and Warnatz, J. (1992) Evaluated kinetic data for combustion modelling. *J. Phys. Chem. Ref. Data* **21,** 411–429.

Boothroyd, R. G. (1971) *Flowing Gas–Solids Suspensions*, p. 14. Chapman and Hall, London.

Coffee, T. P. and Heimerl, J. M. (1981) Transport algorithms for premixed laminar, steady-state flames. *Combust. Flame* **43,** 273–289.

Dorfi, E. A. and Drury, L. O'C. (1987) Simple adaptive grids for 1-D initial value problems. *J. Comp. Phys.* **69,** 175–195.

Embid, P. and Baer, M. (1992) Mathematical analysis of a two-phase mixture theory. *Continuum Mech. Thermodyn.* **4,** 279–312.

Ernst, J., Wagner, H. G. and Zellner, R. (1977) Direct rate measurements for OH + OH = H2O + O in the range 1200–1800 K. *Ber. Bunsenges. Phys. Chem.* **81,** 1270–1275.

Fan, B. and Sichel, M. (1988) A comprehensive model for the structure of dust detonations. *22nd Symp. (Int.) Combust.*, pp. 1741–1750.

Friedlander, S. K. (1977) *Smoke, Dust and Haze*, p. 32. John Wiley and Sons, New York.

Fuchs, N. A. (1964) *The Mechanics of Aerosols*, pp. 30–34. Pergamon Press, New York.

Gardiner, W. C., Mallard, M., McFarland, M., Morinaga, K., Owen, J. H., Rawlins, W. T., Takeyama, T. and Walker, B. G. (1973) Elementary reaction rates from post-induction-period profiles in shock-initiated combustion. *14th Symp. (Int.) Combust.*, pp. 61–75.

Gersum, S. von and Roth, P. (1992) Soot oxidation in high temperature N_2O/Ar mixtures. *24th Symp. (Int.) Combust.*, pp. 999–1006.

Gonthier, K. A. and Powers, J. M. (1996) A numerical investigation of transient detonation in granulated material. Technical Report, Department of Aerospace and Mechanical Engineering, University of Notre Dame, Notre Dame, Indiana, USA.

Ha, M. Y., Choi, B. R. (1994) Numerical study on the combustion of a single carbon particle entrained in a steady flow. *Combust. Flame* **97,** 1–16.

Harten, A. and Lax, P. D. and Leer, B. van (1983) On upstream differencing and Godunov-type schemes for hyperbolic conservation laws. *SIAM Rev.* **25,** 35–61.

Hayashi, A. K. and Fuyoto, T. (1993) Numerical simulation of shock waves through a combustible two-phase. Technical Report, Department of Aeronautical Engineering, Nagoya University, Japan.

Igra, O. and Ben-Dor, G. (1988) Dusty shock waves. *Appl. Mech. Rev.* **41,** 379–437.

Kee, R. J., Warnatz, J. and Miller, J. A. (1983) A FORTRAN computer code package for the evaluation of gas-phase viscosities, conductivities and diffusion coefficients. Technical Report, Sandia National Laboratories, SAND83-8209.

Khasainov, B. A. and Veyssiere, B. (1994) Transformation of detonation modes in hybrid two-phase mixtures. *Proceedings of the International Conference on Combustion Dedicated to the 80th anniversary of Yakov Borisovich Zel'dovich (Zel'dovich Memorial)*, Voronovo, Moscow Region, Russia, Vol. 2, pp. 358–359.

Krazinski, J. L., Buckius, R. O. and Krier, H. (1979) Coal dust flames: a review and development of a model for flame propagation. *Prog. Energy Combust. Sci.* **5,** 31–71.

Krishenik, P. M., Rumanov, E. N. and Shkadinskii, K. G. (1994) Modeling of combustion wave propagation in a carbon dust/gas mixture. *Combust. Flame* **99,** 713–722.

Lebecki, K., Cybulski, K., Śliz, J., Dyduch, Z. and Wolański, P. (1993) Large scale dust explosions research in Poland. *Proceedings of the 14th International Colloquium on the Dynamics of Explosions and Reactive Systems*, Coimbra, Vol. II, E2.4.

Liu, Y. and Vinokur, M. (1989). Upwind algorithms for general thermo-chemical nonequilibrium flows. *27th Aerospace Sciences Meeting, Reno/Nevada*, AIAA-89-0201.

Mack, A., Weber, H.-J. and Roth, P. (1991) A moving grid method applied to one-dimensional non-stationary flame propagation. *Int. J. Num. Meth. Fluids* **13,** 869–882.

Mathur, S., Tondon, P. K. and Saxena, S. C. (1967) Thermal conductivity of binary, ternary and quarternary mixtures of rare gases. *Mol. Phys.* **12,** 569–579.

Peraldi, O., Landry, C., Lee, J. H. and Knystautas, R. (1993) Influence of particle size on dust explosions in a small scale spherical vessel. *Proceedings of the 14th International Colloquium on the Dynamics of Explosions and Reactive Systems*, Coimbra, Vol. II, E2.3.

Petzold, L. R. (1983) *A Description of DASSL: A Differential/Algebraic System Solver*. Amsterdam, North-Holland.

Proust, C. and Veyssiere, B. (1988) Fundamental properties of flames propagating in starch dust–air mixtures. *Combust. Sci. and Tech.* **62,** 149–172.

Roth, P., Brandt, O. and Gersum, S. von (1990) High temperature oxidation of suspended soot particles verified by CO and CO_2 measurements. *23rd Symp. (Int.) Combust.*, pp. 1485–1491.

Sichel, M. (1991) Numerical modeling of heterogeneous detonations. In *Numerical Approaches to Combustion Modeling*, Chap. 14, AIAA Progress in Aeronautics and Astronautics, Vol. 135, pp. 447–449.

Sirignano, W. A. (1993) Fluid dynamics of sprays—1992 Freeman scholar lecture. *J. Fluids Eng.* **115,** 345–378.

Smirnov, N. N. (1988) Combustion and detonation in multi-phase media. Initiation of detonation in dispersed-film systems behind a shock wave. *Int. J. Heat Mass Transfer* **31,** 779–793.

Smirnov, N. N. and Tyurnikov, M. V. (1994) A study of deflagration and detonation in multiphase hydrocarbon–air mixtures. *Combust. Flame* **96,** 130–140.

Stuhmiller, J. H. (1977) The influence of interfacial pressure forces on the character of two-phase flow model equations. *Int. J. Multiphase Flow* **3,** 551–560.

Tsang, W. and Hampson, R. F. (1986) Chemical kinetic data base for combustion chemistry. Part I. Methane and related compounds. *J. Phys. Chem. Ref. Data* **15,** 1087–1279.

Tsuji, Y., Shen, N. Y. and Morikawa, Y. (1989) Numerical simulation of gas–solid flows–I and II. *Technology Reports of the Osaka University* **39,** 233–254.

Warnatz, J. (1977) Berechnung der Flammengeschwindigkeit und der Struktur von laminaren, flachen Flammen, Habilitationsschrift, Darmstadt.

Warnatz, J. (1982) Influence of transport models and boundary conditions on flame structure. In *Numerical Methods in Flame Propagation*. Vieweg, Wiesbaden.

Warnatz, J. (1983) Hydrocarbon oxidation at high temperatures. *Ber. Bunsenges. Phys. Chem.* **87,** 1008–1022.

Warnatz, J. (1984) Rate coefficients in the C/H/O system. In *Combustion Chemistry*, ed. W. C. Gardiner, pp. 197–360. Springer, New York.

Wilke, C. R. (1950) A viscosity equation for gas mixutres. *J. Chem. Phys.* **18,** 517–519.

Yee, H. C. (1987) Upwind and symmetric shock capturing schemes. NASA TM 89464.